



Factors that affect carbothermal synthesis of nanoscale zero-valent iron supported activated carbon and its use as dechlorination agent of hexachlorobenzene

Wei-fang Chen^{a,*}, Weipeng Lu^a, Sijia Zhang^a, Xiaobing Xie^b, Fei-fei He^a, Zai Chen^a

^aSchool of Environment and Architecture, University of Shanghai for Science and Technology, Shanghai 200093, China, Tel. +86-15026671846; Fax: +86-21-55275979; email: chenweifang@usst.edu.cn (W.-f. Chen), Tel./Fax: +86-21-55275979; emails: lwp_1994@163.com (W. Lu), zhangsijia21@usst.edu.cn (S. Zhang), zaichen1993@163.com (Z. Chen), Tel. +86-21-55270697; Fax: +86-21-55275979; email: hff1992@usst.edu.cn (F.-f. He)

^bSchool of International Trade and Economics, University of International Business and Economics, Beijing 100029, China, Tel./Fax: +86-10-64493488; email: handspring@163.com

Received 1 March 2017; Accepted 5 August 2017

ABSTRACT

Starting with sucrose and ferrous chloride, nanoparticles of iron encapsulated in carbon structure were synthesized using a carbothermal method. The effects of carbothermal temperature, treatment time, Fe:sucrose mass ratio on the properties of the nanoscale zero-valent iron supported activated carbon were investigated. Temperatures ranged from 500°C to 1,100°C and treatment time used was 0.5, 1 and 3 h. Mass ratios of Fe and sucrose were 1:2, 1:4 and 1:8, respectively. Materials thus obtained were mostly powdered. X-ray diffraction patterns indicate that zero-valent iron was successfully produced from reduction of iron oxides. Iron was incorporated into the carbon structure. Hexachlorobenzene was employed as the target substance to test the material's application. The optimum synthesis condition which resulted in a more than 95% HCB removal was carbothermal temperature of 700°C, treatment time of 1 h and mass ratio of Fe:sucrose of 1:4.

Keywords: Carbothermal synthesis; Nano zero-valent iron; Synthesis conditions; HCB dechlorination

1. Introduction

Nano zero-valent iron (nZVI) can effectively degrade a wide range of persistent organic and inorganic pollutants, such as chlorinated organic compounds [1,2], heavy metals [3,4] and organic dyes [5] in aqueous streams. Compared with commercial iron powder, nZVI material is renowned for its large surface area and high reactivity. However, due to high surface energy and intrinsic magnetic interaction, bare nZVI tends to aggregate into microscale particles [6]. This agglomeration phenomenon is oftentimes the main reason of reduced efficiency and poor catalytic performance by nZVI [7]. To address this issue, attempts have been made to disperse nZVI particles on porous materials such as resin [8], kaolinite [9], bentonite [10], chitosan [11] and activated

carbon [12]. Among them, the combination of nZVI and activated carbon showed remarkable advantages. Mackenzie et al. [13] observed that activated carbon provided the matrix for controlled deposition of nZVI, thus nZVI showed much less agglomeration and controllable transport properties. Additionally, activated carbon's hydrophobic nature led to concentration of groundwater pollutants in the vicinity of the reactive iron surface [14]. This is especially beneficial for removal of hydrophobic organics.

The synthesis of nZVI supported on a carbon carrier by means of reduction of ferrous or ferric has been carried out in various ways. Most was prepared by a liquid-phase reduction method using salt of borohydride as the reducing agent [15–17]. However, high cost of borohydride and the production of large volume of hydrogen gas made such a process complex and cost-intensive, impeding the scale-up of the process [18]. Carbothermal synthesis of nZVI, as

* Corresponding author.

an alternative method, takes advantage of carbon itself to reduce iron oxides into zero-valent iron and meanwhile provides a hydrophobic carbon support for the Fe⁰ nanoparticles. Zhan et al. [19] employed an aerosol-based process and a subsequent carbothermal reduction to produce spherical carbon-iron nanocomposite. The apparent reaction rate in the dechlorination of TCE by the carbon-iron composite reached 9.2/h at 0.1 wt% Pd/Fe-C ratio where palladium served as a catalyst. Also, part of the carbon was reacted away as CO and CO₂ and a high porosity in iron-carbon composites was introduced allowing the entry of contaminants to reactive sites. The whole process was endothermic and gave only gaseous by-products, so it was potentially scalable to large reactors and continuous processing.

However, the synthesis of activated carbon-zero valent iron composite through carbothermal method is complex and the physical and chemical properties of the particles are easily influenced by synthesis conditions. Zhang et al. [20] reported that size and shape of the products were sensitive to treatment temperature and reaction time. Suman and Orlandi [21] studied the influence of processing parameters on nanomaterials synthesis efficiency by a carbothermal reduction process. The effects of the starting material, temperature and synthesis time, and nitrogen gas flux were investigated. The results showed that a yield of 95% of nano tin dioxide was achieved by carbothermal reduction process using a starting material composed of a mixture of SnO₂:C in molar proportions of 1.5:1 at 1,135°C for 75 min using a N₂ gas flux of 80 cm³/min.

In the current work, sucrose and ferrous salt was employed as starting materials to synthesize a carbon-iron composite. It was expected that sucrose would be carbonized to form a basic carbon structure while ferrous salt was converted to iron oxides and then reduced to elemental iron with carbon as the reducing agent. Fe:sucrose mass ratio, carbothermal temperature and treatment time were varied to investigate the effects of synthesis conditions on the characteristics of final products.

In addition, HCB was employed as the target substance to investigate the pollution removal capacity of thus synthesized materials. Epidemiology studies have shown that HCB is probably human carcinogenic [22]. Short- and long-term exposure could lead to kidney, liver damage and damage in central nervous system. HCB contaminated sites pose long-term serious environmental and health risks because of its persistence. HCB was found in many river sediments and groundwater system in China due to wastewater discharge from chemical plants.

Our objectives were to (1) investigate the effects of treatment temperature, time and Fe:sucrose mass ratio on the physical and chemical properties of the carbothermal products; (2) characterize the relationship between physicochemical properties (iron content, particle size, apparent density, etc.) of the products and synthesis conditions and (3) compare the HCB removal and dechlorination capability of materials synthesized at different conditions.

2. Materials and methods

2.1. Chemicals and materials

Ferrous chloride tetrahydrate (FeCl₂·4H₂O) was purchased from Aladdin Reagent Co., Ltd. (Shanghai, China).

Sucrose, potassium dichromate (K₂Cr₂O₇), 1,5-diphenylcarbazide, acetone and the other reagents (H₃PO₄ and H₂SO₄) were provided by the Sinopharm Group Chemical Reagent Co., Ltd. (Shanghai, China). All the chemicals were used without further purification. Deionized water was used in all preparation.

2.2. Synthesis of nanoscale zero-valent iron supported porous activated carbon

Nanoscale zero-valent iron supported activated carbon (nZVI/AC) was prepared using sucrose and FeCl₂ as precursors. Preliminary tests were conducted to decide experimental conditions (e.g., time of ultrasound dispersion, N₂ purge, etc.). The effects of carbothermal temperature, treatment time and Fe:sucrose ratio on the properties of synthesized materials were then studied in detail.

To investigate the impact of carbothermal temperature, 2.4 g of sucrose was added to 100 mL of FeCl₂ solution (6 g/L as iron), which made a Fe:sucrose ratio of 1:4. The mixture was then dispersed by ultrasound for 15 min and was added to a corundum boat and put in a tube furnace. The tube is purged with N₂ for 10 min before heating. Temperature was ramped up to 500°C, 700°C, 900°C or 1,100°C, respectively, at 5°C/min and kept at the predetermined temperature for an hour and then cooled to room temperature under N₂ atmosphere. Samples thus obtained were named as Fe/C-temperature.

The effect of treatment time was investigated by varying time from 0.5, 1 to 3 h. Carbothermal temperature and Fe:sucrose was set as 700°C and 1:4, respectively. Samples were named as Fe/C-time.

Another factor studied was the Fe:sucrose ratio. Specifically, 2.4 g of sucrose was added to 100 mL of FeCl₂ solution with concentration of iron ranging from 3, 6 and 12 g/L, which corresponded to Fe:sucrose ratio of 1:2, 1:4 and 1:8, respectively. The tests were conducted at carbothermal temperature of 700°C and treatment time of 1 h.

2.3. Characterization and analysis methods

The crystal structure of nZVI/AC was examined with an X-ray diffraction (XRD; D8A A25, Bruker AXS GmbH, Germany) with a high-power Cu Kα radiation at a scanning rate of 8°/min for 2θ from 10° to 80°.

Scanning electron microscope (SEM; S4800, Hitachi, Japan) and transmission electron microscope (TEM) Tecnai G20 (FEI, USA) were used to observe the morphology and microstructure of the materials.

BET surface area and pore-size distribution were determined using nitrogen adsorption method with the 3H-2000PS4 surface analyzer system (Beishide Instrument, China).

Iron contents of nZVI/AC were analyzed using a digestion method [21]. 0.5 g of material was washed at 600°C for 4 h and then digested with 25 mL of concentrated hydrochloric acid. The digestion solutions were analyzed for iron by an atomic absorption spectrophotometer with graphite furnace TAS-990 (Beijing, China).

The apparent density was determined by the ratio of mass to a given volume and particle-size distribution was measured by separation using standard screens with mesh size of 80, 120 and 180.

2.4. Batch experiments on HCB dechlorination

10, 30, 50, 80, 150 or 300 mg of nZVI/AC was added to vials each containing 20 mL of 1 mg/L HCB solution. Initial pH was adjusted to around 6.0. The mixtures were shaken for 8 h at 150 rpm and 25°C. nZVI/AC was then separated from solution by filtration. Both nZVI/AC and filtrate were then extracted for 0.5 h with 20 mL of *n*-hexane and analyzed for HCB.

$$\text{HCB removal efficiency} = \frac{m_0 - m_1}{m_0} \times 100\% \quad (1)$$

$$\text{Percentage of dechlorination} = \frac{m_0 - m_2}{m_0} \times 100\% \quad (2)$$

where m_0 is the initial amount of HCB (mg); m_1 is the residual amount of HCB extracted from solution (mg) and m_2 is the residual amount of HCB extracted from both solution and solid (mg).

HCB analysis was conducted via an Agilent 7890A-5975C gas chromatography-mass spectrometry (Agilent Technologies, USA) equipped with an HP-5MS capillary column [23]. Specifically, 1 μ L of extraction was injected automatically in splitless mode. The temperatures of injector and detector were set at 320°C and 350°C, respectively. Separation was controlled with a temperature program that started at oven temperature at 40°C, held for 5 min, then ramped at 20°C/min to 200°C, and then ramped at 5°C/min to 250°C, held for 2 min.

All tests above were done in triplet. Data given are average with deviation.

3. Results and discussion

3.1. Effects of carbothermal temperature

The temperature of carbothermal treatment is always one of the predominating factors that affect the existing form of species and active performance of nZVI deposited materials [24]. Sucrose and FeCl₂ mixture underwent carbothermal treatment at temperature ranging from 500°C to 1,100°C in this study. Fig. 1 shows the XRD patterns of nZVI/AC by carbothermal treatment at different temperature. All samples showed peaks at 26.3° indicating the existence of graphite carbon [25]. As temperature increased, there was a general increase in the intensity and sharpness of the graphite peak. During carbothermal treatment, solvent first evaporated and then sucrose carbonized to form the basic carbon structure. The increase in graphite intensity may indicate increased aromatization of carbon and graphite matrix of activated carbon is gradually taking shape.

Diffraction peaks at 18.1°, 30.2°, 35.1°, 36.7°, 56.7° and 62.3° are all related to the existence of iron oxide [26]. Peaks at 2 θ of 43°–45° are attributable to pure α -Fe (110) with a body-centered cubic (bcc) crystalline structure, while those at 53.2° and 64.9° can be attributed to Fe(200) [27]. During heating process, iron ions and/or salts were transformed first into iron oxides as solvent evaporated. Zero-valent iron was produced through reduction by the carbonized sucrose. XRD patterns revealed that zero-valent iron (Fe⁰) was present at all temperatures. However, the higher Fe⁰ peak intensities at temperatures 900°C and 1,100°C showed that the crystalline

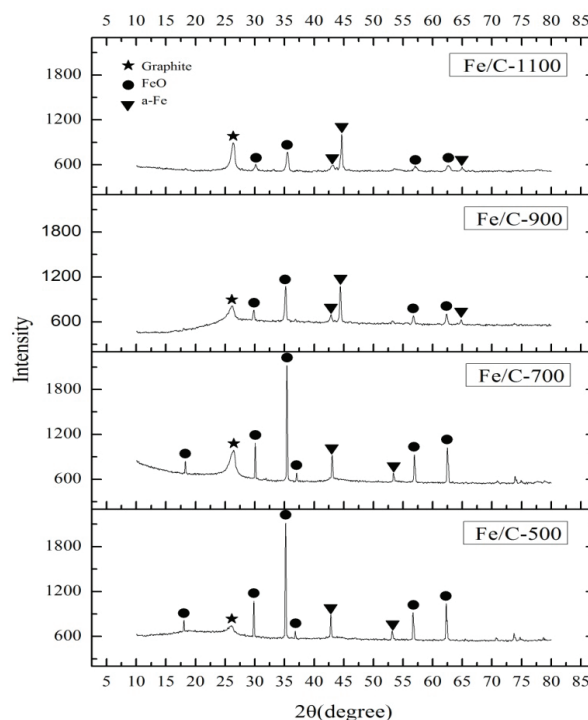


Fig. 1. XRD patterns of nZVI/AC carbothermally synthesized at different temperature.

iron content increased at high temperature. In addition, the increase in Fe⁰ peak was accompanied by the gradual weakening of iron oxide peaks (especially iron oxide peak at 35.7°). It is therefore proposed that, during carbothermal process, iron oxide could be reduced by elemental carbon to form elemental iron while carbon itself was oxidized and gasified as CO and CO₂ as shown in reactions (3)–(5) [19].



Fig. 2 is the SEM images of nZVI/AC samples synthesized at different temperature. These images clearly show the porous nature of the synthesized materials. Also, as temperature increased, larger particles were formed. Fig. 3 is the TEM images. It is evident that roughly spherical nZVI particles were randomly distributed and immobilized inside the carbon structure. The large gray sheet is carbon structure while metal particles are shown as darker clusters. Metal particles in synthesized materials ranged from about 20–50 nm in size indicating that nanoparticles were formed. nZVI particles alone often exhibit a strong tendency to agglomerate and retain chain-like morphology. It seems that when nanoparticles were encapsulated in porous carbon, the agglomeration of nZVI was minimized. Iron particles were separated and presented as individual spherical shaped ones as shown in Fig. 2. Thus, dispersed nanoparticles might lead to good contact with target contaminants and sequential reactions.

Apparent density, iron contents, BET surface area and pore volume were then obtained and listed in Table 1. Apparent densities ranged from 0.46 to 0.66 g/cm³ which is roughly the apparent density observed in commercially available activated carbon.

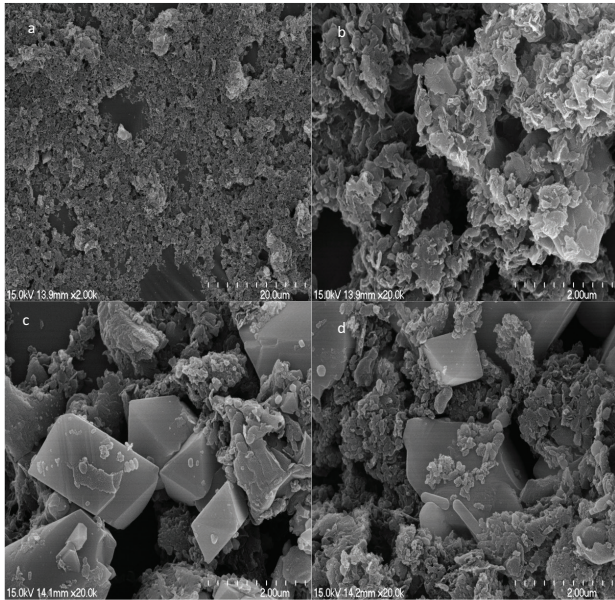


Fig. 2. SEM images of (a) Fe/C-500; (b) Fe/C-700; (c) Fe/C-900 and (d) Fe/C-1,100.

Temperature had great impact on the formation of porosity. As shown in Eqs. (3)–(5), carbon was gasified as CO and CO₂ during the formation of elemental iron. The gasification facilitated the formation of porosity. Fe/C-700 achieved the highest surface area of 313 m²/g and a total pore volume of 0.29 mL/g. However, porosity dropped as temperature increased. Fe/C-900 had a surface area of 236 m²/g while that of Fe/C-1,100 was only 86 m²/g. This could probably be due to the sintering effect at extreme temperature.

Iron content increased as the increase of temperature. More carbon was lost as CO and CO₂ at high temperature thus increases in the percentage of iron in total mass.

Table 2 is the particle-size distribution which is used to judge the granularity of materials. According to American Society for Testing and Materials (ASTM) classification, powdered activated carbon is defined as particles with an 80 mesh sieve (0.18 mm) and smaller [28]. More than 90% of Fe/C-500, Fe/C-700 and Fe/C-900 could pass through 80-mesh, meaning that those are basically powdered materials. By comparison, Fe/C-1,100 had the highest percentage of particles that could be deemed granular. Still, more than 80% of the particles were powder. The results corresponded well with what was observed from SEM images. As shown in Fig. 2, Fe/C-500 was mostly small particles while larger ones were observed at higher temperatures. This could be caused by sintering at high temperature. Smaller carbon particles aggregated to form larger ones as temperature increased.

In water and wastewater treatment, powdered and granular materials have difference usage. For instance, powdered

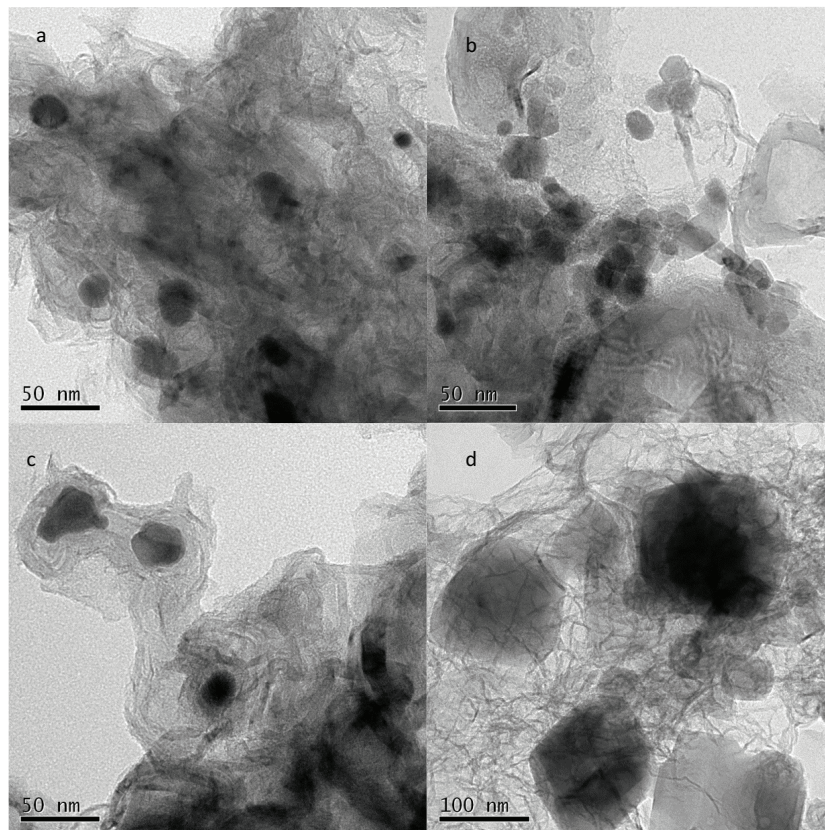


Fig. 3. TEM images of (a) Fe/C-500; (b) Fe/C-700; (c) Fe/C-900 and (d) Fe/C-1,100.

Table 1

Apparent density, iron content, BET surface area and pore volume of nZVI/AC synthesized at different temperature (treatment time 1 h, Fe:sucrose 1:4)

Samples	Apparent density (g/cm ³)	BET surface area (m ² /g)	Total pore volume (cm ³ /g)	Iron content (mg/g)
Fe/C-500	0.66 ± 0.05	282 ± 12.0	0.21 ± 0.03	249 ± 3.1
Fe/C-700	0.64 ± 0.05	313 ± 8.0	0.29 ± 0.02	275 ± 2.5
Fe/C-900	0.57 ± 0.03	236 ± 6.0	0.25 ± 0.04	383 ± 2.2
Fe/C-1,100	0.46 ± 0.05	86 ± 7.0	0.14 ± 0.03	482 ± 2.5

Table 2

Particle-size distribution (percentage of total mass) of nZVI/AC synthesized at different temperature

Standard screen size (mesh)	Fe/C-500	Fe/C-700	Fe/C-900	Fe/C-1,100
>80	4.90	9.21	11.25	19.60
80–120	12.50	17.85	12.63	12.60
120–180	32.85	28.40	22.50	20.58
<180	49.75	44.54	53.62	47.58

materials are not commonly used in a fixed bed system, due to the high head loss that would occur. Instead, they are generally added directly to the water streams or as an enhancement for other process units (membrane treatment, filtration, etc.) [29]. Being largely powder, nZVI/AC thus synthesized could easily be adopted in a direct dosing scenario. Due to its smaller particle size, powdered activated carbon could be superior in regard to adsorption kinetics and might be more efficient compared with granular activated carbon.

nZVI/AC obtained was then tested for HCB removal. To exclude the effect of particle size on HCB removal, only particles of size 80–200 mesh were used. nZVI/AC was proven to be capable of HCB dechlorination [30]. Therefore, studies here mainly focused on the investigation of extent of dechlorination. Figs. 4(a) and (b) are HCB removal efficiency and percentage of dechlorination at different dosage. Overall, HCB removal increased with the increase of dosage. At the same dosage, HCB removal follows the order of Fe/C-700 > Fe/C-900 > Fe/C-1,100 > Fe/C-500. Dechlorination follows roughly the same order though the differences between samples are smaller. In summary, the removal of HCB is a combination of adsorption and dechlorination. For instance, 96% of HCB was removed at dosage of 8 g/L for Fe/C-700. Of that, 45% was dechlorinated while the rest 51% was adsorbed. The amount of dechlorination varied. Fe/C-1,100 resulted in 39.96% dechlorination although it contained a much higher amount of iron (482 mg/g). However, surface area of Fe/C-1,100 is smaller thus may lead to weaker adsorption. This proves that a right combination of surface porosity and iron content seems to be needed for optimum removal. This is understandable since HCB has to be adsorbed first to come into contact with reactive iron to be dechlorinated.

3.2. Effects of carbothermal treatment time

Based on results from tests on carbothermal temperature, Fe/C-700 appears to manifest the highest HCB removal.

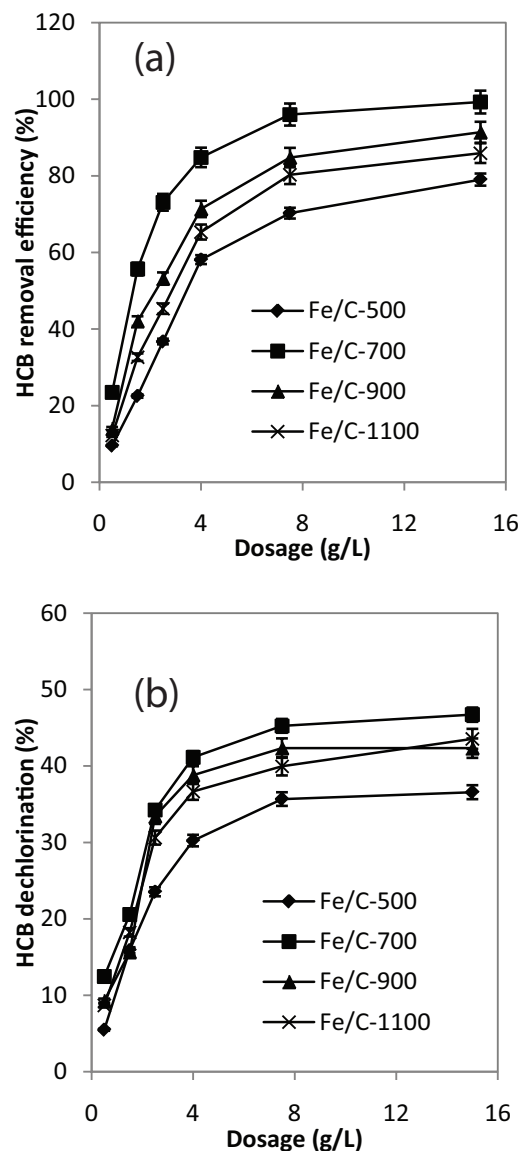


Fig. 4. HCB removal by nZVI/AC carbothermally synthesized at different temperature: (a) HCB removal efficiency and (b) HCB dechlorination.

Therefore, in the investigation of the influence of treatment time, carbothermal temperature was set at 700°C while treatment time varied from 0.5, 1 to 3 h. XRD patterns of resulted

samples are shown in Fig. 5. XRD patterns are quite similar and treatment time did not seem to have any significant effects on the material's crystal structure.

Apparent density, iron content, BET surface area and total pore volumes were also compared as shown in Table 3 while Table 4 lists the particle-size distribution. There are slight increases in all parameters as treatment time increased from 0.5 to 1 h. However, the increases are no longer statistically significant when extending the treatment time further to 3 h. The same is with particle-size distribution. Granularity did not change significantly after treatment time of 1 h.

Fig. 6 compares the HCB removal efficiency and dechlorination by nZVI/AC obtained by different treatment time. The results matched well with the results from characterization. There is significant improvement both in HCB removal and dechlorination at treatment time of 0.5 and 1 h. But the differences between 1 and 3 h are negligible.

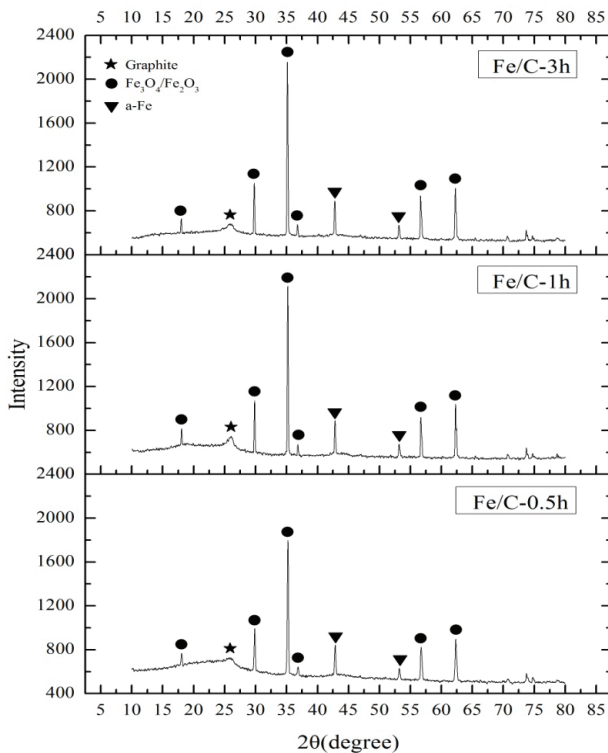


Fig. 5. XRD patterns of nZVI/AC carbothermally synthesized at different treatment time.

Table 3
Apparent density, iron content, BET surface area and pore volume of nZVI/AC synthesized at different treatment time (treatment temperature 700°C, Fe:sucrose 1:4)

Samples	Apparent density (g/cm ³)	BET surface area (m ² /g)	Total pore volume (cm ³ /g)	Iron content (mg/g)
Fe/C-0.5 h	0.56 ± 0.02	232 ± 5.2	0.21 ± 0.03	253 ± 3.5
Fe/C-1 h	0.64 ± 0.05	313 ± 8.0	0.29 ± 0.02	275 ± 2.5
Fe/C-3 h	0.62 ± 0.04	320 ± 4.5	0.28 ± 0.03	282 ± 4.2

3.3. Effects of mass ratio

Three mass ratios of Fe:sucrose were studied in order to evaluate the effects of the composition of starting material. The carbothermal temperature and treatment time were kept the same at 700°C and 1 h.

Table 4
Particle-size distribution (percentage of total mass) of nZVI/AC synthesized at different treatment time

Standard screen size (mesh)	Fe/C-0.5 h	Fe/C-1 h	Fe/C-3 h
>80	6.65	9.21	10.50
80–120	13.80	17.85	22.90
120–180	27.70	28.40	21.10
<180	51.65	44.54	45.50

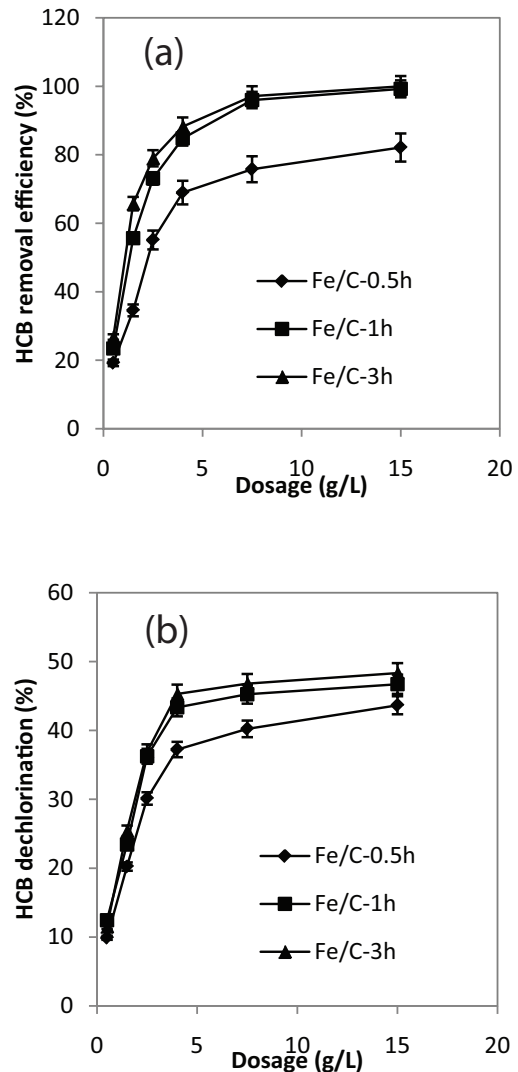


Fig. 6. HCB removal by nZVI/AC carbothermally synthesized at different treatment time: (a) HCB removal efficiency and (b) HCB dechlorination.

Fig. 7 is the XRD patterns of samples of different mass ratio from 1:2, 1:4 to 1:8. The effect of Fe:sucrose ratio on the crystal structure of the zero-valent iron was obvious. Sharp diffraction peaks at 43° – 45° of α -Fe (110) crystal plane was observed of sample with 1:8 ratio, suggesting good crystalline degree [31]. At the same time, peaks of iron oxides almost disappeared at this Fe:sucrose ratio indicating probably a more thorough reduction of iron oxides to Fe^0 . In contrast, XRD patterns of Fe:sucrose of 1:2 and 1:4 are quite similar with strong peaks of both iron oxides and Fe^0 . The difference could be attributed to the fact that at ratio of 1:8, more carbon was available thus more complete reduction.

Apparent density, BET surface area, total pore volume and iron content differed at different Fe:sucrose ratio as shown in Table 5. Less carbon in the starting material resulted in a final product that is more porous and higher in iron content as BET surface area, total pore volume and iron content all increased as Fe:sucrose ratio varied from 1:8 to 1:2. Su et al. [12] studied the synthesis of zero-valent iron/activated carbon composite from agricultural waste (coir pith). They concluded that iron-containing compound acted as facilitator of carbon activation. The high porosity at low carbon content

(high starting Fe percentage) in this study could be a result of enhanced activation by excessive iron compounds. In addition, although sample of Fe:sucrose = 1:2 are more porous. It still showed the highest apparent density. This could be because of the high iron content since iron is denser.

Particle-size distribution (Table 6), on the other hand, shows that less carbon led to smaller particles as more than 92% of particles at Fe:sucrose = 1:2 could be counted as powder. By comparison, less than 80% of particles at Fe:sucrose ratio 1:8 is powder. Sucrose provided the supporting activated carbon structure for iron or iron oxides. Higher carbon ratio at the start may mean that more materials were available to form carbon structure thus higher granularity.

Samples synthesized from various Fe:sucrose ratio was also tested for their HCB removal and dechlorination. Figs. 8(a) and (b) are the results. At the same dosage, HCB removal increased as Fe:C sucrose ratio decreased. That is, the highest removal were with sample at Fe:sucrose = 1:2. However, its removal efficiency was only slightly better than that of Fe:sucrose = 1:4. As far as cost was concerned, iron chemicals were much more expensive than sucrose, the extra expenses on iron chemicals for the small improvement in HCB removal may not be justified.

Sample from Fe:sucrose of 1:8 obtained the highest dechlorination. As shown in XRD results, Fe:sucrose of 1:8 resulted in a material that is mostly composed of Fe^0 thus high dechlorination. At all dosages, more than half of the HCB removal could be attributed to dechlorination. In their synthesis of iron-carbon nanocomposite, Zhang et al. [32] observed that zero-valent iron was encapsulated in an iron oxide shell. The iron oxide shell could seriously affect the reactivity of zero-valent iron inside. Therefore, although sample synthesized at Fe:sucrose of 1:8 showed much higher dechlorination, the effect may not be long lasting once Fe^0 was oxidized in air. This oxidation process is not obvious in this study since HCB removal test was carried out right after synthesis. Studies are ongoing as for the aging effect of materials.

Taking into consideration the chemical cost and Fe^0 oxidation, it seems that Fe:sucrose of 1:4 is the optimal Fe:sucrose ratio.

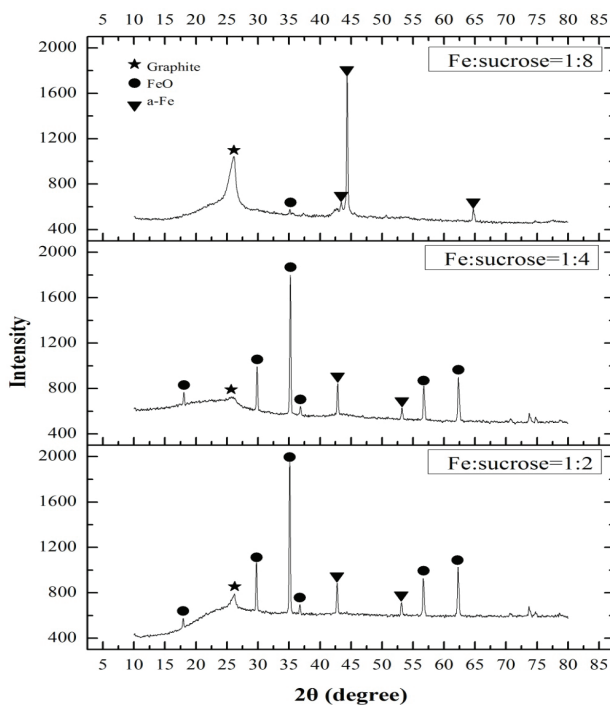


Fig. 7. XRD patterns of nZVI/AC carbothermally synthesized at different Fe:sucrose mass.

Table 5

Apparent density, iron content, BET surface area and pore volume of nZVI/AC synthesized at different Fe:sucrose ratio (treatment time 1 h, temperature 700°C)

Samples	Apparent density (g/cm^3)	BET surface area (m^2/g)	Total pore volume (cm^3/g)	Iron content (mg/g)
1:2	0.75 ± 0.02	328 ± 7.5	0.38 ± 0.03	573 ± 5.5
1:4	0.64 ± 0.05	313 ± 8.0	0.29 ± 0.02	275 ± 2.5
1:8	0.56 ± 0.03	132 ± 5.6	0.21 ± 0.03	132 ± 3.2

Table 6

Particle-size distribution (percentage of total mass) of nZVI/AC synthesized at different Fe:sucrose ratio

Standard screen size (mesh)	1:2	1:4	1:8
>80	7.82	9.21	21.25
80–120	13.19	17.85	14.40
120–180	31.87	28.40	25.70
<180	47.12	44.54	38.65

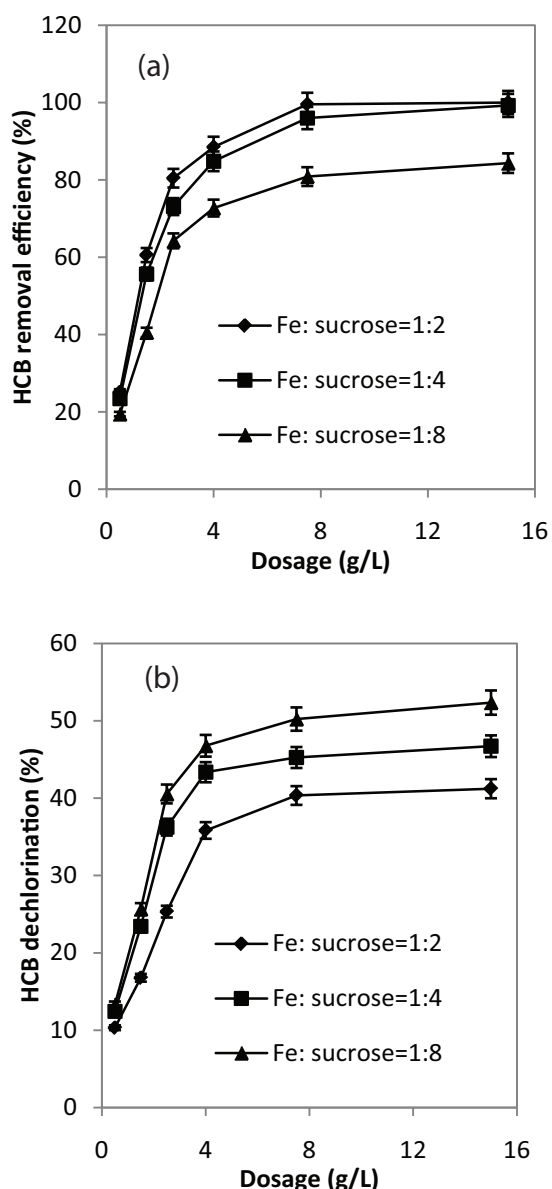


Fig. 8. HCB removal by nZVI/AC carbothermally synthesized at different Fe:sucrose ratio: (a) HCB removal efficiency and (b) HCB dechlorination.

4. Conclusions

nZVI/AC was successfully prepared via a carbothermal method and the effects of carbothermal temperature, treatment time and mass ratio of Fe:sucrose on the characteristics of the final products and HCB removal were investigated. Powdered porous activated carbons were synthesized at all conditions. Properties such as surface area, pore volume, iron content and particle-size distribution is directly related to the synthesis conditions. High temperature resulted in higher iron content but low porosity. Treatment time no longer had significant effect when it reached longer than 1 h. High Fe:sucrose ratio (less carbon) led to high porosity and high iron content. As far as HCB removal is concerned, it is a combination of adsorption and dechlorination by Fe^0 . Therefore, a synthesis

condition that result in a material that showed a balance in porosity and iron content may be better. Overall, HCB removal results showed that the optimum conditions are: temperature 700°C , treatment time 1 h and Fe:sucrose ratio 1:4.

Acknowledgments

This work was supported by Shanghai Natural Science Foundation (14ZR1428900); China Postdoctoral Science Foundation (2017M611590), Returned Overseas Chinese Scholars, State Education Ministry (SEM2013) and Shanghai Committee of Science and Technology (13230502300).

References

- [1] D. Kaifas, L. Malleret, N. Kumar, W. Fetimi, M. Claeys-Bruno, M. Sergent, P. Doumenq, Assessment of potential positive effects of nZVI surface modification and concentration levels on TCE dechlorination in the presence of competing strong oxidants, using an experimental design, *Sci. Total Environ.*, 481 (2014) 335–342.
- [2] J.Y. Ahn, C. Kim, H.S. Kim, K.Y. Hwang, I. Hwang, Effects of oxidants on in situ treatment of a DNAPL source by nanoscale zero-valent iron: a field study, *Water Res.*, 107 (2016) 57–65.
- [3] A.M. Azzam, S.T. El-Wakeel, B.B. Mostafa, M.F. El-Shahat, Removal of Pb, Cd, Cu and Ni from aqueous solution using nano scale zero valent iron particles, *J. Environ. Chem. Eng.*, 4 (2016) 2196–2206.
- [4] P.P. Huang, Z.F. Ye, W.M. Xie, Q. Chen, J. Li, Z.C. Xu, M.S. Yao, Rapid magnetic removal of aqueous heavy metals and their relevant mechanisms using nanoscale zero valent iron (nZVI) particles, *Water Res.*, 47 (2013) 4050–4058.
- [5] C.D. Raman, S. Kanmani, Textile dye degradation using nano zero valent iron: a review, *J. Environ. Manage.*, 177 (2016) 341–355.
- [6] T. Phenrat, N. Saleh, K. Sirk, R.D. Tilton, G.V. Lowry, Aggregation and sedimentation of aqueous nanoscale zerovalent iron dispersions, *Environ. Sci. Technol.*, 41 (2007) 284–290.
- [7] L. Alidokht, A.R. Khataee, A. Reyhanitabar, S. Oustan, Reductive removal of Cr(VI) by starch-stabilized Fe^0 nanoparticles in aqueous solution, *Desalination*, 270 (2011) 105–110.
- [8] A. Toli, K. Chalastara, C. Mystrioti, A. Xenidis, N. Papassiopi, Incorporation of zero valent iron nanoparticles in the matrix of cationic resin beads for the remediation of Cr(VI) contaminated waters, *Environ. Pollut.*, 214 (2016) 419–429.
- [9] Z.X. Chen, T. Wang, X.Y. Jin, Z.L. Chen, M. Megharaj, R. Naidu, Multifunctional kaolinite-supported nanoscale zero-valent iron used for the adsorption and degradation of crystal violet in aqueous solution, *J. Colloid Interface Sci.*, 398 (2013) 59–66.
- [10] A. Soliemanzadeh, M. Fekri, The application of green tea extract to prepare bentonite-supported nanoscale zero-valent iron and its performance on removal of Cr(VI): effect of relative parameters and soil experiments, *Microporous Mesoporous Mater.*, 239 (2017) 60–69.
- [11] T.Y. Liu, Z.L. Wang, L. Zhao, X. Yang, Enhanced chitosan/ Fe^0 -nanoparticles beads for hexavalent chromium removal from wastewater, *Chem. Eng. J.*, 189–190 (2012) 196–202.
- [12] Y.F. Su, Y.L. Cheng, Y.H. Shih, Removal of trichloroethylene by zerovalent iron/activated carbon derived from agricultural wastes, *J. Environ. Manage.*, 129 (2013) 361–366.
- [13] K. Mackenzie, S. Bleyl, A. Georgi, F.D. Kopinke, Carbon-iron-an Fe/AC composite-as alternative to nano-iron for groundwater treatment, *Water Res.*, 46 (2012) 3817–3826.
- [14] S. Bleyl, F.D. Kopinke, K. Mackenzie, Carbo-iron⁰—synthesis and stabilization of $\text{Fe}(0)$ -doped colloidal activated carbon for in situ groundwater treatment, *Chem. Eng. J.*, 191 (2012) 588–595.
- [15] P. Singh, P. Raizada, S. Kumari, A. Kumar, D. Pathania, P. Thakur, Solar-Fenton removal of malachite green with novel Fe^0 -activated carbon nanocomposite, *Appl. Catal., A*, 476 (2014) 9–18.

- [16] F.L. Fu, W.J. Han, S.J. Huang, B. Tang, M. Hu, Removal of Cr(VI) from wastewater by supported nanoscale zero-valent iron on granular activated carbon, *Desal. Wat. Treat.*, 51 (2013) 2680–2686.
- [17] X.Q. Wu, Q. Yang, D.C. Xu, Y. Zhong, K. Luo, X.M. Li, H.B. Chen, G.M. Zeng, Simultaneous adsorption/reduction of bromate by nanoscale zerovalent iron supported on modified activated carbon, *Ind. Eng. Chem. Res.*, 52 (2013) 12574–12581.
- [18] L.B. Hoch, E.J. Mack, B.W. Hydutsky, J.M. Hershman, J.M. Skluzacek, T.E. Mallouk, Carbothermal synthesis of carbon-supported nanoscale zero-valent iron particles for the remediation of hexavalent chromium, *Environ. Sci. Technol.*, 42 (2008) 2600–2605.
- [19] J.J. Zhan, B. Sunkara, J.J. Tang, Y.Q. Wang, J.B. He, G.L. McPherson, V.T. John, Carbothermal synthesis of aerosol-based adsorptive-reactive iron-carbon particles for the remediation of chlorinated hydrocarbons, *Ind. Eng. Chem. Res.*, 50 (2011) 13021–13029.
- [20] J.C. Zhang, W.Q. Shen, Z.W. Zhang, D.Y. Pan, M.H. Wu, One-step pyrolysis route to C/Fe₃O₄ hybrids from EDTA ferric sodium salt, *Mater. Lett.*, 64 (2010) 817–819.
- [21] P.H. Suman, M.O. Orlandi, Influence of processing parameters on nanomaterials synthesis efficiency by a carbothermal reduction process, *J. Nanopart. Res.*, 13 (2011) 2081–2088.
- [22] J.F. Jarrell, A. Gocmen, D. Akyol, R. Brant, Hexachlorobenzene exposure and the proportion of male births in Turkey 1935–1990, *Reprod. Toxicol.*, 16 (2002) 65–70.
- [23] X. Nie, J.G. Liu, Rapid degradation of hexachlorobenzene by micron Ag/Fe bimetal particles, *J. Environ. Sci.*, 25 (2013) 473–478.
- [24] Y. Wang, H. Sun, X. Duan, H.M. Ang, M.O. Tade, S. Wang, A new magnetic nano zero-valent iron encapsulated in carbon spheres for oxidative degradation of phenol, *Appl. Catal., B*, 172–173 (2015) 73–81.
- [25] X.S. Lv, J. Xu, G.M. Jiang, J. Tang, X.H. Xu, Highly active nanoscale zero-valent iron (nZVI)-Fe₃O₄ nanocomposites for the removal of chromium(VI) from aqueous solutions, *J. Colloid Interface Sci.*, 369 (2012) 460–469.
- [26] P. Hu, S.G. Zhang, H. Wang, D.A. Pan, J.J. Tian, Z. Tang, A.A. Volinsky, Heat treatment effects on Fe₃O₄ nanoparticles structure and magnetic properties prepared by carbothermal reduction, *J. Alloys Compd.*, 509 (2011) 2316–2319.
- [27] M.A. Salam, O. Fageeh, S.A. Al-Thabaiti, A.Y. Obaid, Removal of nitrate ions from aqueous solution using zero-valent iron nanoparticles supported on high surface area nanographenes, *J. Mol. Liq.*, 212 (2015) 708–715.
- [28] Q. Lu, G.A. Sorial, Adsorption of phenolics on activated carbon—impact of pore size and molecular oxygen, *Chemosphere*, 55 (2004) 671–679.
- [29] J. Altmann, A.S. Ruhl, F. Zietzschmann, M. Jekel, Direct comparison of ozonation and adsorption onto powdered activated carbon for micropollutant removal in advanced wastewater treatment, *Water Res.*, 55 (2014) 185–193.
- [30] W.F. Chen, L. Pan, L.F. Chen, Q. Wang, C.C. Yan, Dechlorination of hexachlorobenzene by nano zero-valent iron/activated carbon composite: iron loading, kinetics and pathway, *RSC Adv.*, 4 (2014) 46689–46696.
- [31] B. Cao, Q.L. Liu, D. Zhang, Synthesis and characterization of porous carbon/Fe nanocomposite, *J. Inorg. Mater.*, 25 (2010) 457–462.
- [32] X. Zhang, S. Lin, X.Q. Lu, Z.L. Chen, Removal of Pb(II) from water using synthesized kaolin supported nanoscale zero-valent iron, *Chem. Eng. J.*, 163 (2010) 243–248.